

11 FEB 1958

18895
11 FEB 1958
Copy 226
RM L58A06

NACA RM L58A06

TECH LIBRARY KAFB, NM
D144747

NACA

RESEARCH MEMORANDUM

HEAT TRANSFER MEASURED ON A FLAT-FACE CYLINDER-FLARE

CONFIGURATION IN FREE FLIGHT AT MACH NUMBERS

FROM 1.6 TO 2.7

By Dorothy B. Lee and Andrew G. Swanson

Langley Aeronautical Laboratory
Langley Field, Va.

CLASSIFIED DOCUMENT

This material contains information affecting the National Defense of the United States within the meaning of the espionage laws, Title 18, U.S.C., Secs. 793 and 794, the transmission or revelation of which in any manner to an unauthorized person is prohibited by law.

NATIONAL ADVISORY COMMITTEE FOR AERONAUTICS

WASHINGTON
February 3, 1958

~~CONFIDENTIAL~~

7827

Classification corrected (i.e. changed to Unclassified)

to: NASATech Pub Announcement #14
(OFFICER GRADE/POSITION CHANGE)

By: 3 Mar 60
NAME AND GRADE

NC
(GRADE OF OFFICER MAKING CHANGE)

23 Feb 61
DATE



NATIONAL ADVISORY COMMITTEE FOR AERONAUTICS

RESEARCH MEMORANDUM

HEAT TRANSFER MEASURED ON A FLAT-FACE CYLINDER-FLARE
CONFIGURATION IN FREE FLIGHT AT MACH NUMBERS
FROM 1.6 TO 2.7

By Dorothy B. Lee and Andrew G. Swanson

SUMMARY

Heat-transfer measurements were obtained on a flat-face cylinder-flare configuration in free flight to a Mach number of 2.7, corresponding to a free-stream Reynolds number per foot of 16.71×10^6 . Temperatures were measured at 12 stations on the configuration. Comparisons of theoretical and measured heating rates indicate that the flow was probably laminar on the flat face and turbulent on the cylinder and flare. Very low heating rates occurred on the cylinder just back of the flat face where separation probably existed.

INTRODUCTION

Aerodynamic heating on missiles at supersonic and hypersonic speeds is currently being investigated by the Langley Pilotless Aircraft Research Division by means of rocket-propelled models in free flight. It has been suggested that the flat-face cylinder-flare configuration might be an efficient reentry shape for ballistic missiles. The heating characteristics of the flat face have been measured recently in free flight and the results are presented in references 1 to 3 to a Mach number of 14.6.

In order to study the heating characteristics of the complete flat-face cylinder-flare configuration, a flight test utilizing a two-stage rocket system has been conducted. (Because of malfunctioning of the ground equipment the second stage failed to fire, however.) Aerodynamic heating data were obtained to a Mach number of 2.7. The data are presented herein for free-stream Mach numbers between 1.6 and 2.7 corresponding to free-stream Reynolds numbers per foot between 10.62×10^6 and 16.71×10^6 .

The flight test was conducted at the Langley Pilotless Aircraft Research Station at Wallops Island, Va., on August 13, 1957. The second-stage rocket motor (JATO, 1.52-KS-33,550, XM19 "Recruit") used in the present investigation was made available by the U. S. Air Force.

SYMBOLS

a	speed of sound, ft/sec
c_p	specific heat of air at constant pressure, Btu/lb-°F
c_w	specific heat of wall material, Btu/lb-°F
g	gravitational constant, 32.2 ft/sec ²
M	Mach number
N_{Pr}	Prandtl number
N_{St}	Stanton number, $\frac{c_w \rho_w T \frac{dT}{dt}}{(T_{aw} - T_w) g c_p \rho_l V_l}$
p	pressure, lb/sq in.
q	heating rate, Btu/(sq ft)(sec)
R	Reynolds number
r	radius of nose, 0.1458 ft (1.75 in.)
T	temperature, °R unless otherwise noted
t	time, sec
V	velocity, ft/sec
x	distance along nose surface from stagnation point, ft
ρ	density of air, slugs/cu ft
ρ_w	density of wall material, lb/cu ft
τ	thickness of wall, ft

Subscripts:

aw	adiabatic wall
w	wall condition
t	stagnation
∞	free stream
l	local
1	condition at measured station at stagnation point
2	stagnation condition behind normal shock

MODEL, INSTRUMENTATION, AND TEST TECHNIQUE

Model

The model, as shown in figure 1, was a body of revolution 138.74 inches long having a flat-face cylinder-flare test nose. The flare section of the nose was a 15° half-angle conical frustum. Figure 1 is a sketch showing pertinent details and dimensions of the model. Also shown are details of the test nose and the locations of the thermocouples.

Photographs of the nose are presented in figures 2 and 3. Figure 3 shows the test nose after final polishing just prior to firing. (Small waviness of the surface near the weld joint, evident in figure 2, is considerably magnified by the light falling on the surface. Since the flow over the cylinder and flare was turbulent, as is shown subsequently, it is believed that the waviness had a negligible effect on the data presented.)

The flat-face section of the nose was fabricated from 0.059-inch-thick Inconel and the skin along the cylindrical and flare section was fabricated from 0.031-inch-thick Inconel. The flat face was backed by a support block of micarta 0.50 inch thick.

Joining the nose with the rocket motor was a conical frustum having a total angle of 9.5° which housed most of the telemetering equipment. The skin of this section was of 0.06-inch-thick Inconel.

The external surface of the nose was very carefully polished, with particular attention being given to the flat-face and cylindrical section of the nose. Polishing began with the use of No. 600 emery paper and

grade number 14 diamond compound and progressed through finer grades of the compound. The face and the first 2 inches of the cylinder were finished with grade number 1 diamond compound (0- to 2-microinch particles). Measurements with an interference-type microscope indicated a surface roughness of 0 to 3 microinches on the flat face, 0 to 5 microinches on the cylindrical section, and 10 to 15 microinches on the flare section of the nose.

In order to achieve stabilization of the model, a conical frustum having a total angle of 20° was attached to the rear of the sustainer rocket motor.

Instrumentation

Measurements of twelve thermocouples, three accelerometers, and one pressure pickup were transmitted from the model during the flight by means of a six-channel telemeter. The thermocouples, made of No. 30 gage chromel-alumel wire, were spot-welded to the inner surface of the Inconel skin at the stations indicated in figure 1.

During flight, three standard voltages and the outputs of six thermocouples were commutated on each of two telemeter channels at a rate such that each measurement was recorded about 10 times per second. The three standard voltages, which were chosen equivalent to the lowest, midrange, and the highest temperatures anticipated served as an inflight check calibration of the thermocouple telemetering system.

Measurements from three accelerometers, one longitudinal, one normal, and one transverse, were telemetered from the model during flight. One pressure orifice was located on the flare 1.5 inches from the cylinder-flare junction.

Other instrumentation consisted of ground-based radar units for measuring model velocity and for obtaining the position of the model in space. Atmospheric conditions and wind data were measured to an altitude of 21,400 feet by means of a radiosonde launched near the time of flight and tracked by Rawin set AN/GMD-1A. Velocity data were obtained by means of a CW Doppler radar set and were corrected for wind from rawinsonde data.

Test

The propulsion system consisted of two stages of solid-propellant rocket motors, the booster stage being a Nike M5 JATO rocket motor and the sustainer being an XM19 Recruit.

~~CONFIDENTIAL~~

Figure 4 shows the complete assembly on the launcher just prior to firing with a protective covering over the nose to protect it from salt spray. The model combination was launched at an angle of 60° above the horizontal and reached a maximum velocity of 2,992 feet per second at the time of the first-stage burnout. The Recruit motor was to be fired by a delay squib, ignited at launching. Because of a short circuit in the ground firing leads to the sustainer rocket motor, the second stage did not ignite after the booster burned out but remained attached to the booster and coasted upwards with decreasing Mach number instead of separating from the booster and accelerating to an anticipated Mach number of 7.

Time histories of altitude, free-stream velocity, and free-stream Mach number are shown in figure 5(a) and free-stream temperature, density, and Reynolds number per foot are shown in figure 5(b).

RESULTS AND DISCUSSION

Skin Temperatures

Representative curves of the skin temperatures measured on the flat face, cylinder, and flare of the nose during flight are shown in figures 6(a) to 6(c) to indicate general trends and magnitudes that occurred. The measured inside temperatures are presented along with the outside temperatures which were computed from the inside temperatures by the one-dimensional analysis method of reference 4. Because of the low-heating rates, the differences between the inside and the outside skin temperatures did not exceed 25° F. The temperature at thermocouple location No. 5 was so low that there was a negligible difference between the outside and the inside skin temperature. This location was 0.5 inch from the flat face on the cylinder and apparently was in a region of separated flow.

The difference between inside and outside temperatures was less at the cylinder and flare stations than at the flat-face stations because the heating rates were lower at these stations and also the skin of the cylinder and flare was thinner than that of the flat face. Table I presents the values of faired outside temperatures for the times when the temperatures began to increase (1.7 sec) until the rate of temperature rise became small.

A distribution of outside skin temperatures around the nose is presented in figure 7 for a few times during the flight when the booster was firing and during a 1-second period of coast after burnout of the booster. It should be noted that the lines drawn in figure 7 from station to station at the various times are not meant to be fairings but are merely for

identification purposes. It can be seen that the temperatures on the flat face increased most rapidly near the edge of the face. On the cylinder, the temperatures were very low at the first station, were highest at the middle of the cylinder, and then, as would be expected for either laminar or turbulent flow, decreased with distance along the body. The temperatures were similar at all flare stations and higher than on the cylinder. The large temperature gradient which existed near the first thermocouple on the cylinder indicated the possibility of large conduction effects. Calculations, however, showed that the influence of conduction on the heating rates was always less than 2.5 percent except at thermocouple No. 4 on the flat face at times 4.0 and 4.6 seconds when the influence was as large as 8 percent.

Heat Transfer

Time histories of aerodynamic heat transferred to the skin as obtained by the method of reference 4 are shown in figure 8. This method determines heat transfer from calculated outside wall temperatures.

The experimental heat rate at the stagnation point is compared in figure 8(a) with Fay and Riddell's theory for laminar stagnation point heat transfer (ref. 5) which was also used in references 1 to 3 at high Mach numbers. The rate of change of velocity with x at the stagnation point, which must be known in order to apply this theory, was obtained from a flat-face pressure distribution for a Mach number of 1.5 as given in Maccoll and Codd (ref. 6) and is discussed in reference 1. This pressure distribution gives $\frac{r}{a_t} \left(\frac{dV}{dx} \right)_t = 0.3$ which was assumed to be invariant with Mach number.

The agreement between heat-transfer measurements and theory is generally good. Based on preliminary tests, it is believed that negligible heat loss to the micarta backing occurred at the low temperatures encountered by this model; therefore the presence of the backing would not affect the comparison between theory and experiment.

A distribution of the experimental rate of heating along the flat face divided by the experimental heat rate at the stagnation point is presented in figure 9(a) to show the variation of the heating across the flat face. Also plotted on figure 9(a) are curves obtained from the Lees and Stine and Wanlass theories (refs. 7 and 8, respectively) as ratios in each case of their own stagnation values. These curves, taken from reference 1, are based on the same pressure distribution for a Mach number of 1.5 as mentioned previously. (It should be noted that these theories are evaluated by slope and integral procedures which, on this nose shape at

least, are difficult to determine exactly, and they should be used therefore to indicate trends rather than precise levels.) The experimental heating rates across the face are also plotted in figure 9(b) as ratios of measured heating rates to theoretical stagnation point heating rates (Fay and Riddell (ref. 6)) along with the aforementioned theories of Lees and Stine and Wanlass.

In general, the experimental distributions are lower in level but similar in trend to the distributions based on the laminar theories. At the stagnation point, the measurements varied from 0.75 to 1.1 times the stagnation point theory. The trends and levels of the data of figure 9 indicate the probability that laminar flow existed over the flat face. In this connection, it is interesting to note that the incompressible momentum thickness at the stagnation point was calculated to be about 210 microinches which is large in comparison with the surface roughness of 0 to 3 microinches. The maximum local Reynolds number, based on momentum thickness, at the edge of the face, was 334 at 3.5 seconds ($M = 2.7$).

Figure 10 shows the distribution over the entire configuration as the ratio of local heating to the theoretical stagnation point values (ref. 5) for $t = 2.1$ seconds ($M = 1.58$) and $t = 4.6$ seconds ($M = 2.44$). The figure shows approximately the range of q/q_t which occurred at the cylinder and flare measurement stations, although the two times presented do not include the maximum and minimum values for every station. It can be seen that the heating on the cylinder and flare ranged from much greater to much less than the theoretical stagnation point heating rate during the test. It should be noted that the relative heating to face and sides or flare is a strong function of Mach number. For instance, in reference 3 at a Mach number of about 14, the cylinder heating is only approximately 10 percent of stagnation point heating.

The experimental heating rates along the cylinder and flare are shown in figures 11(a) and 11(b). They are compared with computed theoretical heating rates using values of N_{St} from Van Driest's theory. (See ref. 9.) The calculations assumed free-stream static pressures on the cylinder and theoretical sharp cone static pressures on the flare. Details of the determinations of local conditions and computations of theoretical heating rates are given in the appendix. The local Reynolds numbers used to compute theoretical heating rates were based on the length along the surface from the stagnation point.

Beginning with the earliest time presented, the cylindrical experimental data are lower than the turbulent theory and then show better agreement as peak Mach number is approached and for the rest of the times shown. The flare experimental data show remarkably good agreement with the turbulent theory throughout the flight test.

The theory at $M = 1.99$ ($t = 2.5$ sec) was also computed by using a pressure distribution over a flat-nosed cylinder obtained from unpublished wind-tunnel data at $M = 2.00$. (See appendix and fig. 12.) These pressure data indicated that a lower than free-stream static pressure existed over the forward portion of the cylinder. This reduced pressure noticeably modifies the theory and brings turbulent theory and experiment into fairly close agreement. It is believed that the data at all Mach numbers would be brought into similar agreement if the proper pressure distributions were applied to the theoretical calculations.

The very low heating rates obtained from thermocouple No. 5 just behind the corner of the flat face probably result from separated flow in this region. (Shadowgraphs (fig. 13) obtained with the aforementioned unpublished data indicated probability of separation behind the corner of a flat-nosed cylinder for flow conditions similar to those of this test.) The modification of the pressure distribution to the laminar-flow theory for the data at $M = 1.99$ (2.51 sec) indicates the possibility should be considered that the flow was attached but laminar; it is believed, however, that laminar separation is the more valid assumption. It should be noted that, if the influence of conduction along the skin had been considered in reducing the data, the experimental heating rates at this station would have been lower than the data presented by about 2.5 to 8 percent.

Note that the theoretical heat-transfer rates are not greatly different between the cylinder and flare because the local conditions of M and R (see table II) and thus the heat-transfer coefficients are not greatly different. The difference shown is due mainly to the change in $T_{aw} - T_w$ caused by the different levels of skin temperature between the cylinder and flare. (Computed outside wall temperatures were used in calculating theoretical heating rates. Percentage difference in measured wall temperatures between cylinder and flare were of the same order as the differences in experimental heating rates.)

CONCLUSIONS

A rocket-propelled model was flight tested to a Mach number of 2.7 with which temperature measurements were made on a flat-face cylinder-flare configuration. Comparison of the heating rates derived from these temperature histories with theoretical calculations indicates the following:

1. Heating rates at the stagnation point agreed fairly well with theory for laminar heating at the stagnation point.

2. Distribution of heating across the flat face showed agreement with laminar theory. The heating rates across the face were slightly lower in terms of heating at the stagnation point than those predicted by the theories of Lees and of Stine and Wanlass.

3. On the cylinder the heating rates were in fair agreement with turbulent flat-plate theory when the local flow conditions were based on the local static pressure being equal to the free-stream static pressure. The use of a measured static-pressure variation for one Mach number at which data were reduced brought theory and experiment into close agreement.

4. The experimental heating rates on the flare were in excellent agreement throughout the test with turbulent flat-plate theory when theoretical sharp cone pressures on the flare and at Reynolds numbers based on surface length from the stagnation point were assumed.

5. The experimental heating rates were very low on the cylinder just behind the corner of the flat face in a region where separated flow probably existed.

Langley Aeronautical Laboratory,
National Advisory Committee for Aeronautics,
Langley Field, Va., December 10, 1957.

APPENDIX

LOCAL CONDITIONS ON CYLINDER AND FLARE

In general, the static pressure along the cylinder was assumed to be the free-stream static pressure. As was shown in the discussion, this assumption was not entirely valid. However, no pressure distributions for this exact configuration and only meager data for flat-faced cylinders alone are available. In order to determine the effects on the heat-transfer data of changes in pressure distribution, local conditions along a cylinder were obtained by using unpublished data from a wind-tunnel test at $M = 2.0$ obtained on flat-faced cylinders at a Reynolds number comparable to those of this test. This distribution is shown in figure 12. The total pressure at the measurement locations on the cylinder was assumed in all cases to be the total pressure behind the normal shock. The total-pressure loss across the cylinder-flare juncture was assumed to be that across a two-dimensional shock at the Mach number on the cylinder. Total pressure along the flare was assumed to be constant.

Local conditions of Mach number, temperature, and density were then obtained from the ratios of local static pressure to the total pressure and from total temperature.

The assumption of sharp cone theoretical static pressures on the flare is believed to be valid for this test on the basis of the pressure measurements obtained on the flare. Figure 14 shows a time history of the measured flare pressures compared with computed theoretical pressures using both sharp cone and wedge theories at local cylinder conditions. It is apparent that the measured pressures are in good agreement with the pressures obtained using sharp cone theory. (Of course, the occurrence of the three-dimensional static pressures on the flare may be unique to the conditions of this test. Also it was noted, for this test at least, that changes from three- to two-dimensional static pressures had small effect on the theoretical heating rates.)

Local heating rates were computed from the relation $q = N_{St}(gc_p \rho_l V_l)(T_{aw} - T_w)$. The theory of reference 9 was used to determine N_{St} for laminar and turbulent flow at local conditions with Reynolds number based on surface length from the stagnation point. Adiabatic-wall temperatures were computed using recovery factors equal to $N_{Pr}^{1/2}$ and $N_{Pr}^{1/3}$ for laminar and turbulent flow, respectively, on the cylinder and flare.

Table II shows local parameters at the times presented in the report.

REFERENCES

1. Stoney, William E., Jr., and Swanson, Andrew G.: Heat Transfer Measured on a Flat-Face Cylinder in Free Flight at Mach Numbers Up to 13.9. NACA RM L57E13, 1957.
2. Bland, William M., Jr., Swanson, Andrew G., and Kolenkiewicz, Ronald: Free-Flight Aerodynamic-Heating Data at Mach Numbers Up to 10.9 on a Flat-Face Cylinder. NACA RM L57K29, 1958.
3. Rumsey, Charles B., and Lee, Dorothy B.: Heat-Transfer Measurements in Free Flight At Mach Numbers Up to 14.6 on a Flat-Faced Conical Nose With a Total Angle of 29°. NACA RM L57L03, 1958.
4. Hill, P. R.: A Method of Computing the Transient Temperature of Thick Walls From Arbitrary Variation of Adiabatic-Wall Temperature and Heat-Transfer Coefficient. NACA TN 4105, 1957.
5. Fay, J. A., and Riddell, F. R.: Stagnation Point Heat Transfer in Dissociated Air. Res. Note 18, AVCO Res. Lab., June 1956.
6. Maccoll, J. W., and Codd, J.: Theoretical Investigation of the Flow Around Various Bodies in the Sonic Region of Velocities. British Theoretical Res. Rep. No. 17/45, B. A. R. C. 45/19, Ministry of Supply, Armament Res. Dept., 1945.
7. Lees, Lester: Laminar Heat Transfer Over Blunt-Nosed Bodies at Hypersonic Flight Speeds. Jet Propulsion, vol. 26, no. 4, Apr. 1956, pp. 259-269.
8. Stine, Howard A., and Wanlass, Kent: Theoretical and Experimental Investigation of Aerodynamic-Heating and Isothermal Heat-Transfer Parameters on a Hemispherical Nose With Laminar Boundary Layer at Supersonic Mach Numbers. NACA TN 3344, 1954.
9. Van Driest, E. R.: The Problem of Aerodynamic Heating. Aero. Eng. Rev., vol. 15, no. 10, Oct. 1956, pp. 26-41.

TABLE I. - CALCULATED OUTSIDE TEMPERATURES

Time, sec	Calculated outside temperatures, °F, for x/r of -											
	0	0.286	0.643	0.857	1.286	1.857	2.429	3.143	3.714	4.286	4.857	5.714
	Corresponding to thermocouple numbers -											
	1	2	3	4	5	6	7	8	9	10	11	12
1.7	75	74	75	75	73	73	85	86	88	86	88	88
1.9	77	77	78	78	75	76	89	90	91	92	95	97
2.1	81	81	81	82	75	82	96	97	98	103	108	109
2.3	84	85	86	88	76	91	105	105	106	117	124	127
2.5	90	91	92	97	77	106	118	118	117	136	146	150
2.7	97	100	101	108	79	124	138	134	133	165	172	178
2.9	108	112	114	123	80	147	162	156	151	200	203	210
3.1	124	126	131	142	81	174	189	182	174	237	240	248
3.3	142	143	152	164	83	201	219	209	199	275	281	286
3.4	151	151	162	175	83	216	234	223	210	294	301	304
3.5	161	160	171	184	84	230	250	234	224	312	320	321
3.6	169	168	179	194	84	243	266	246	235	327	337	336
3.8	182	182	193	211	85	268	292	268	255	353	367	364
4.0	194	194	206	225	87	288	314	286	271	375	388	388
4.2	203	206	216	237	88	306	332	303	285	393	406	408
4.4	213	217	225	248	89	320	347	318	297	408	419	423
4.6	220	225	234	256	90	332	359	329	308	420	431	434
4.8	227	232	241	264	92	342	369	339	317	429	439	443
5.0	233	239	249	271	93	350	376	348	326	437	444	450
5.4	243	249	262	281	96	361	388	361	342	444	449	459
5.8	250	258	272	289	100	367	394	370	353	445	448	461
6.2	258	264	279	294	103	370	399	375	359	442	443	458
6.6	262	268	285	298	107	370	399	380	363	435	435	453
7.0	265	271	290	300	110	367	397	381	364	427	425	445

TYPE B

TYPE B

TABLE II.- LOCAL CONDITIONS

(a) On cylinder ($p_2 = p_\infty$)

Time, sec	M_2	T_2	R_2 per ft
2.1	1.51	539.5	9.74×10^6
2.5	1.78	571.3	10.43
2.9	2.00	615.5	10.32
3.5	2.14	655.2	9.74
4.0	2.09	639.6	9.39
4.6	2.02	616.5	9.07

(b) On flare

Time, sec	M_2	T_2	R_2 per ft
2.1	1.23	604.7	9.45×10^6
2.5	1.49	646.9	11.04
2.9	1.68	709.3	11.40
3.5	1.79	765.4	11.04
4.0	1.75	743.5	10.54
4.6	1.70	712.0	10.05

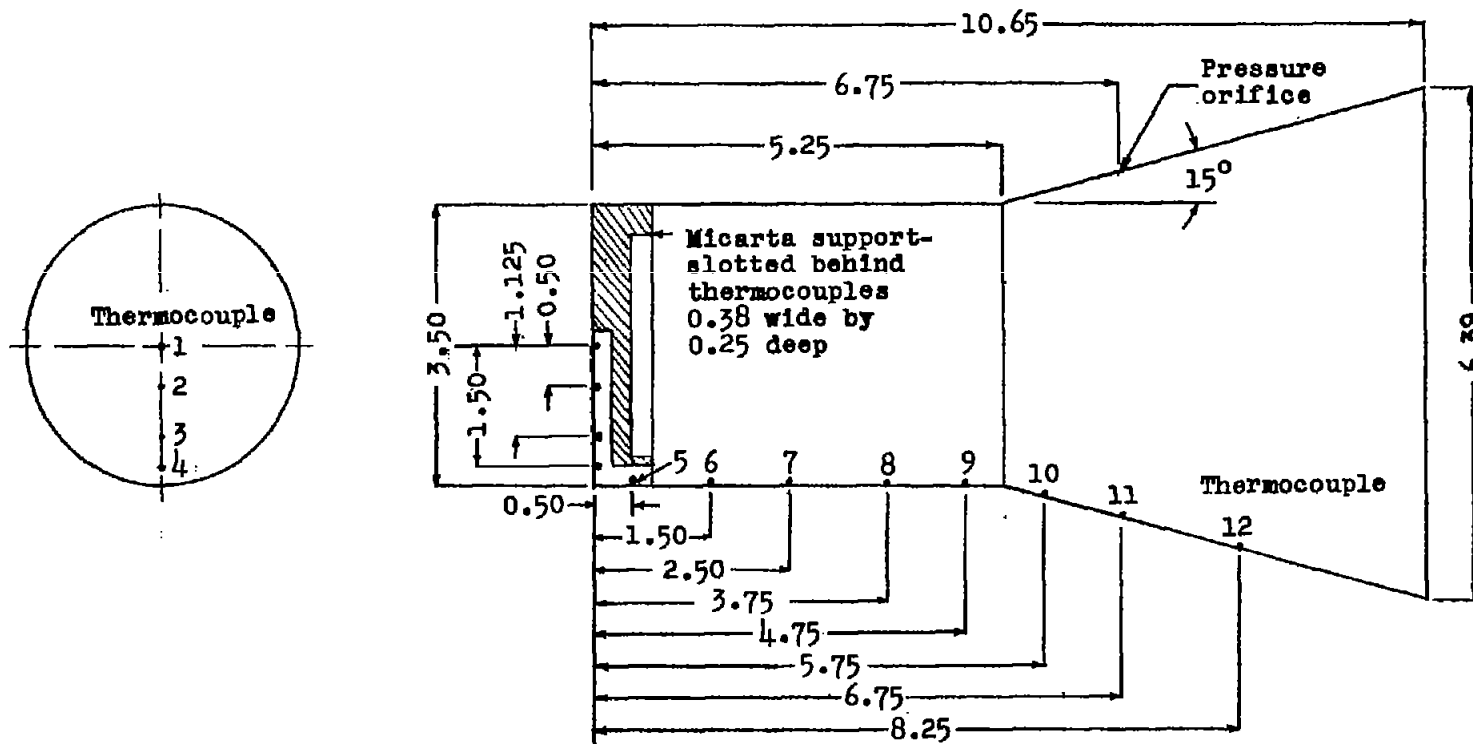
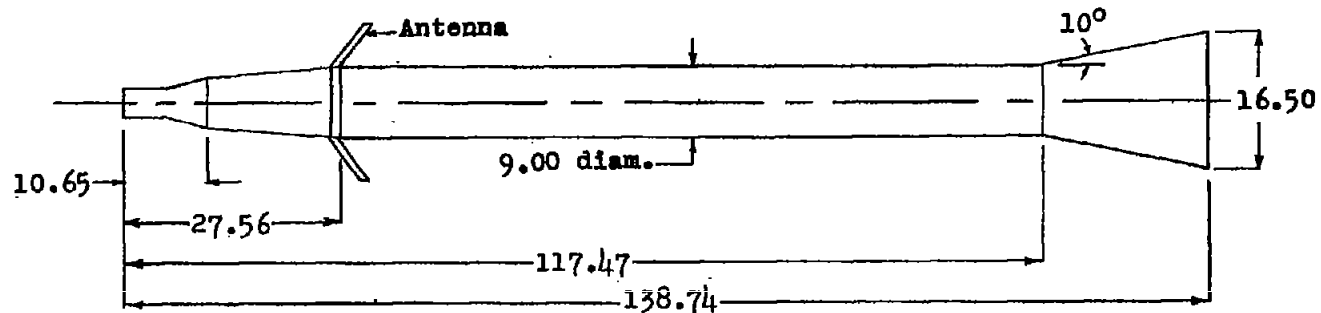


Figure 1.- Drawing of model and nose. Dimensions are in inches.

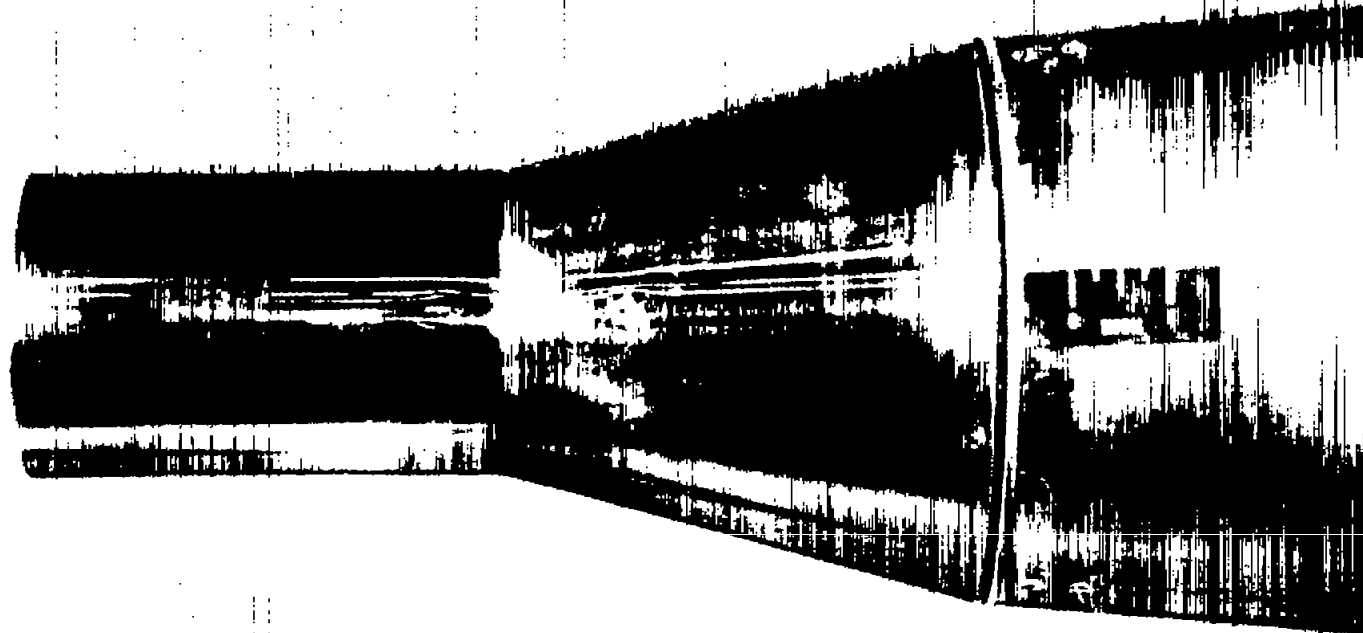


Figure 2.- Photograph of flat-face nose.

L-57-3313



Figure 3.- View of nose on model. — L-57-3543

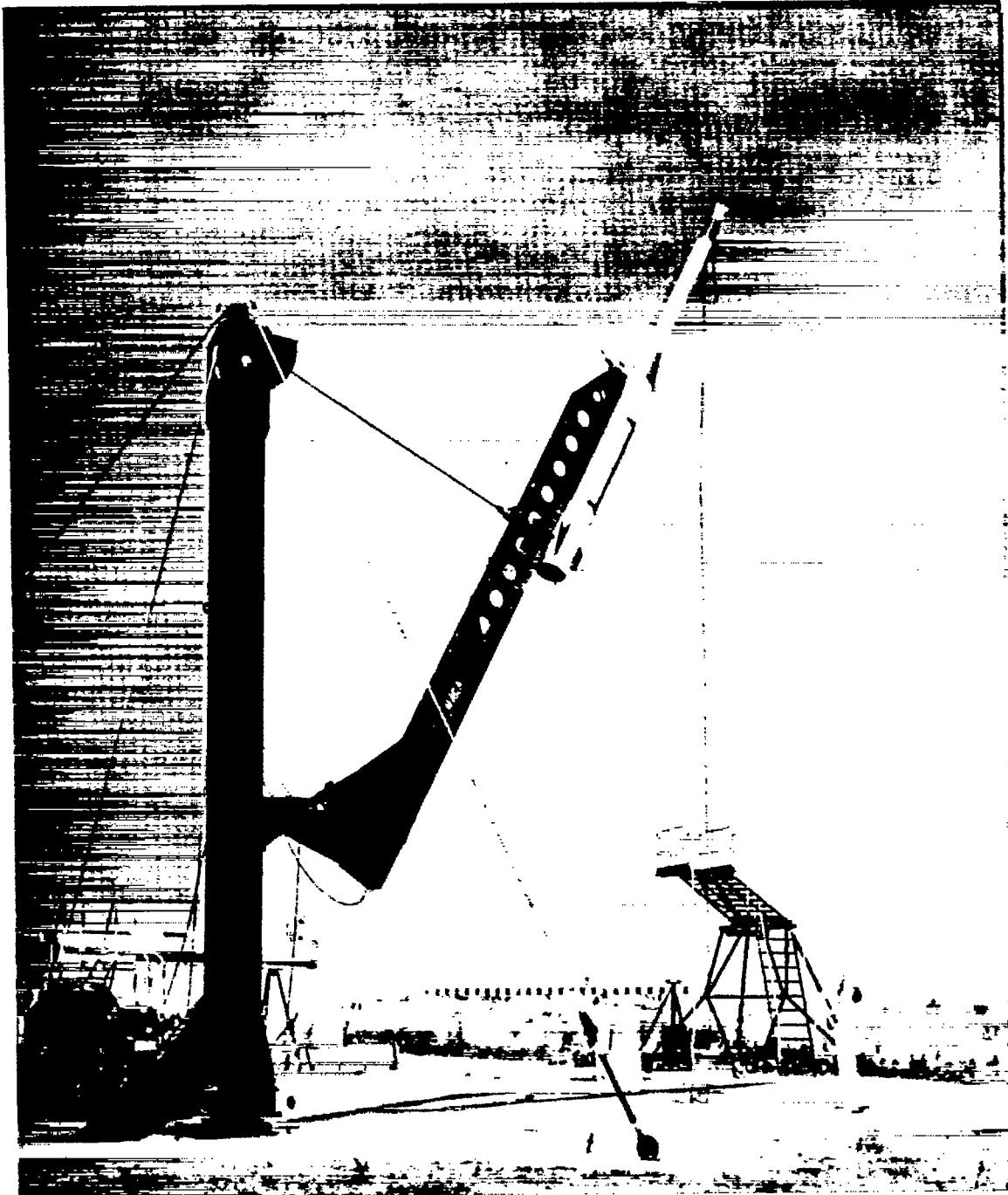
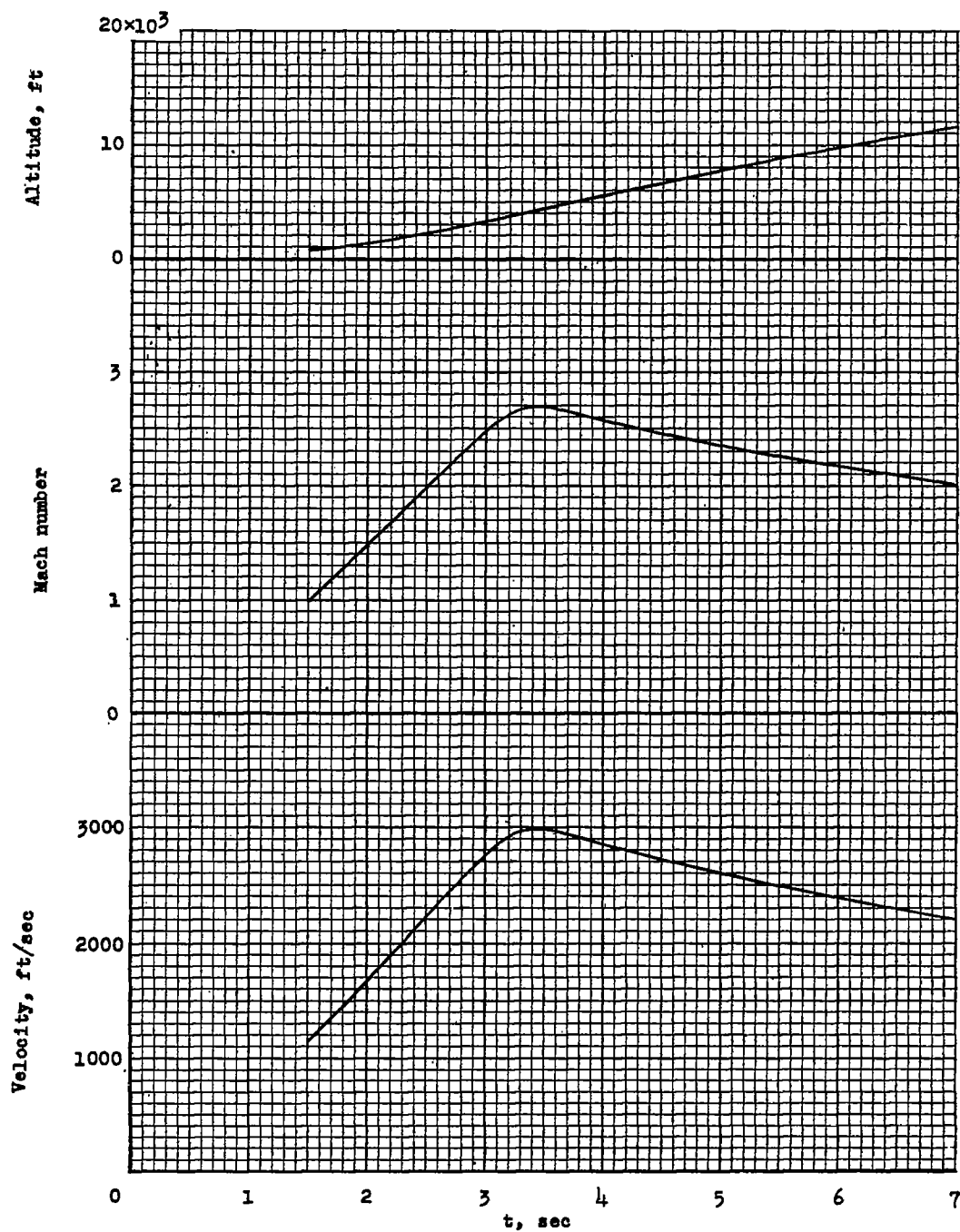
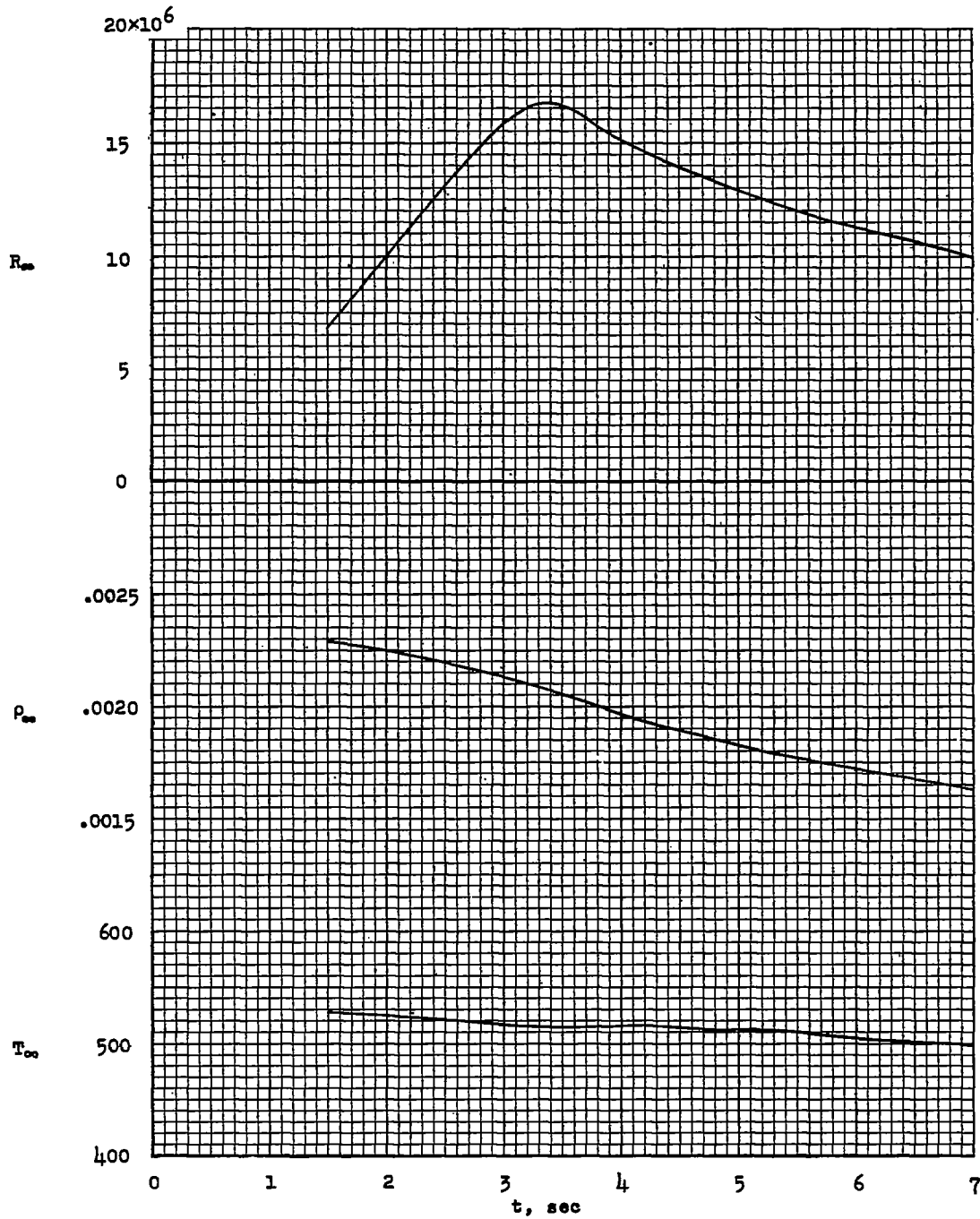


Figure 4.- Model and booster on launcher. L-57-3540



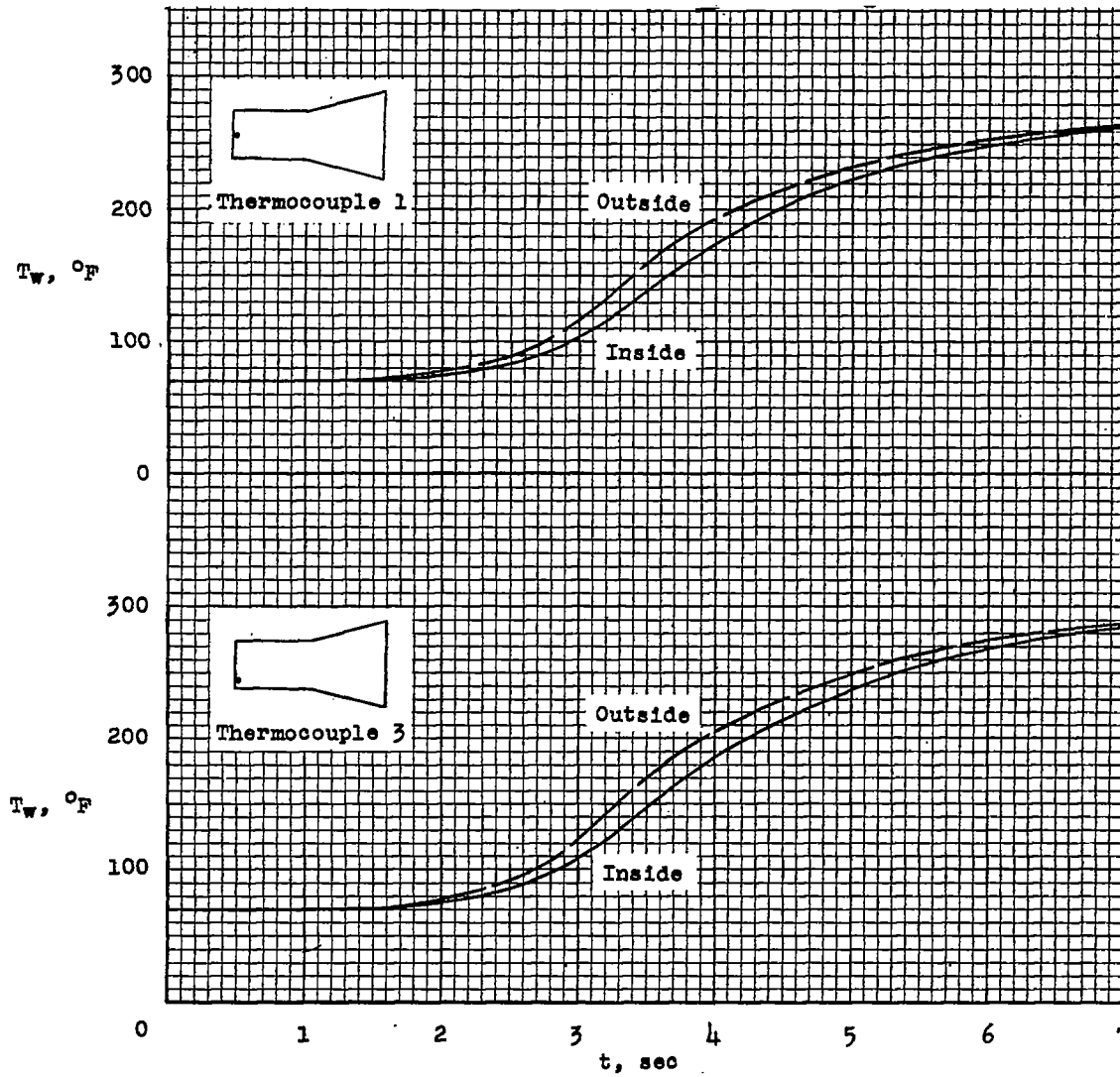
(a) Altitude, Mach number, and velocity.

Figure 5.- Flight conditions.



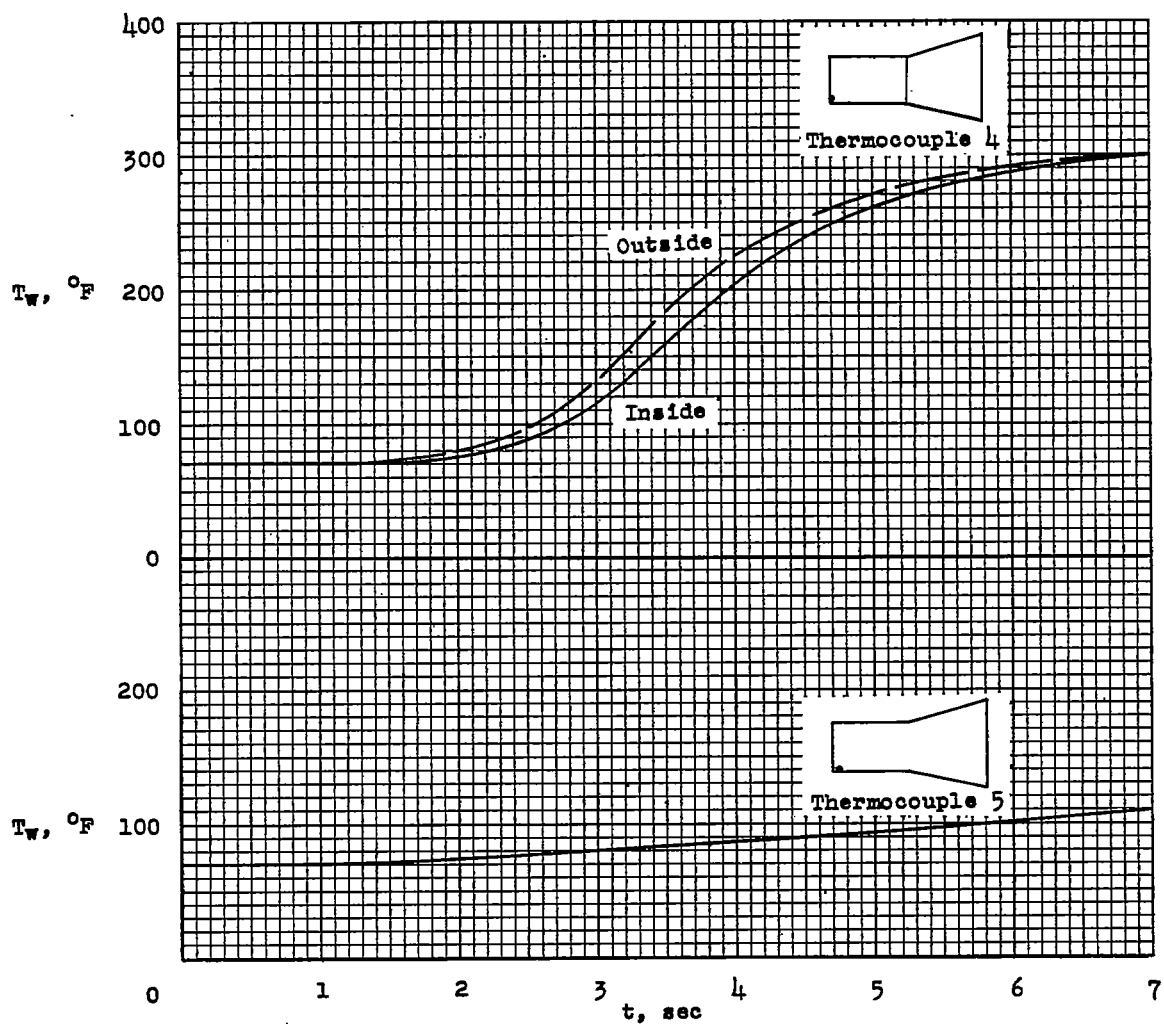
(b) Free-stream Reynolds number per foot, density, and temperature.

Figure 5.- Concluded.



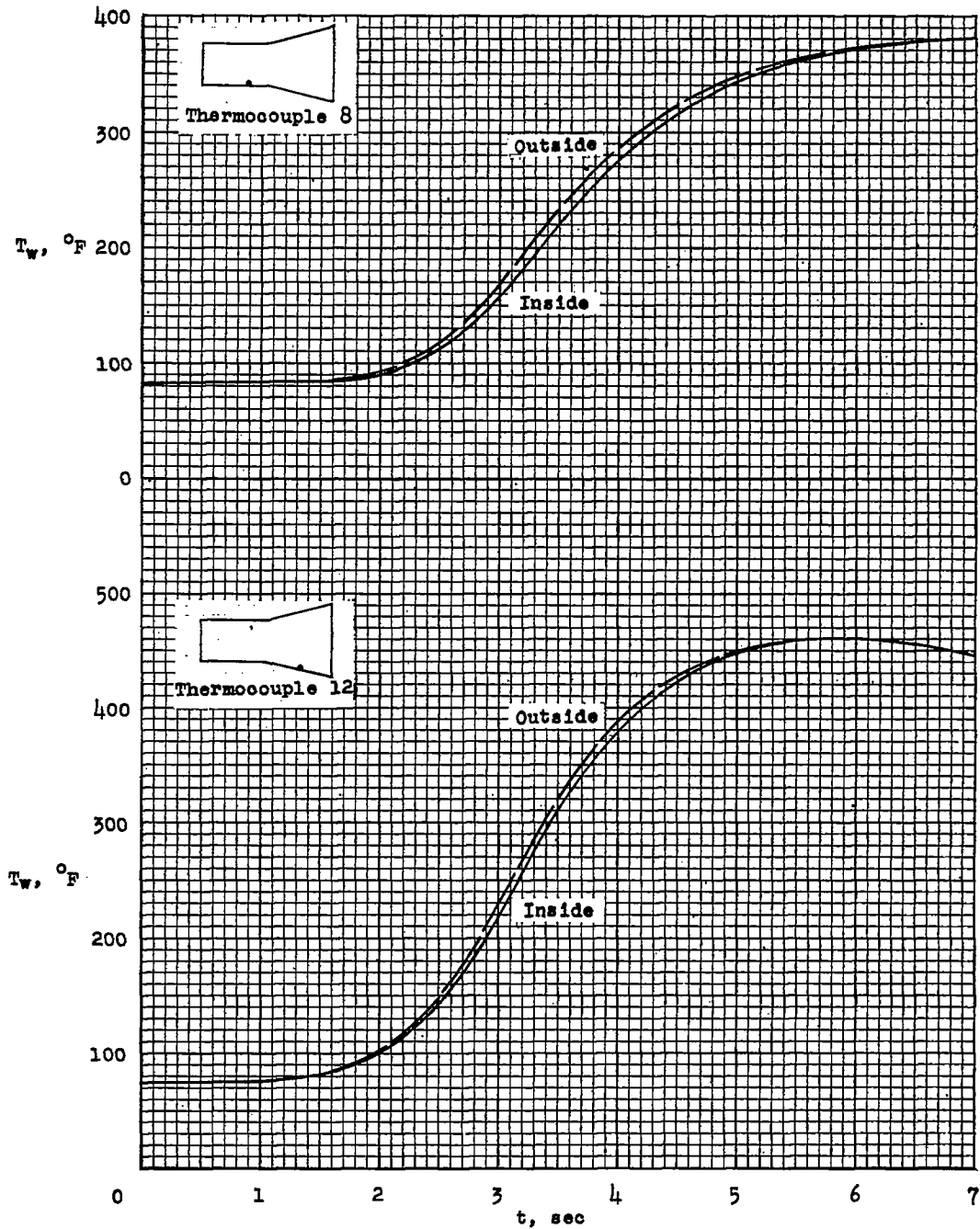
(a) Temperatures on the flat face.

Figure 6.- Typical inside and outside temperatures along the nose.



(b) Temperatures on the flat face and cylinder.

Figure 6.- Continued.



(c) Temperatures on the cylinder and flare.

Figure 6.- Concluded.

CONFIDENTIAL

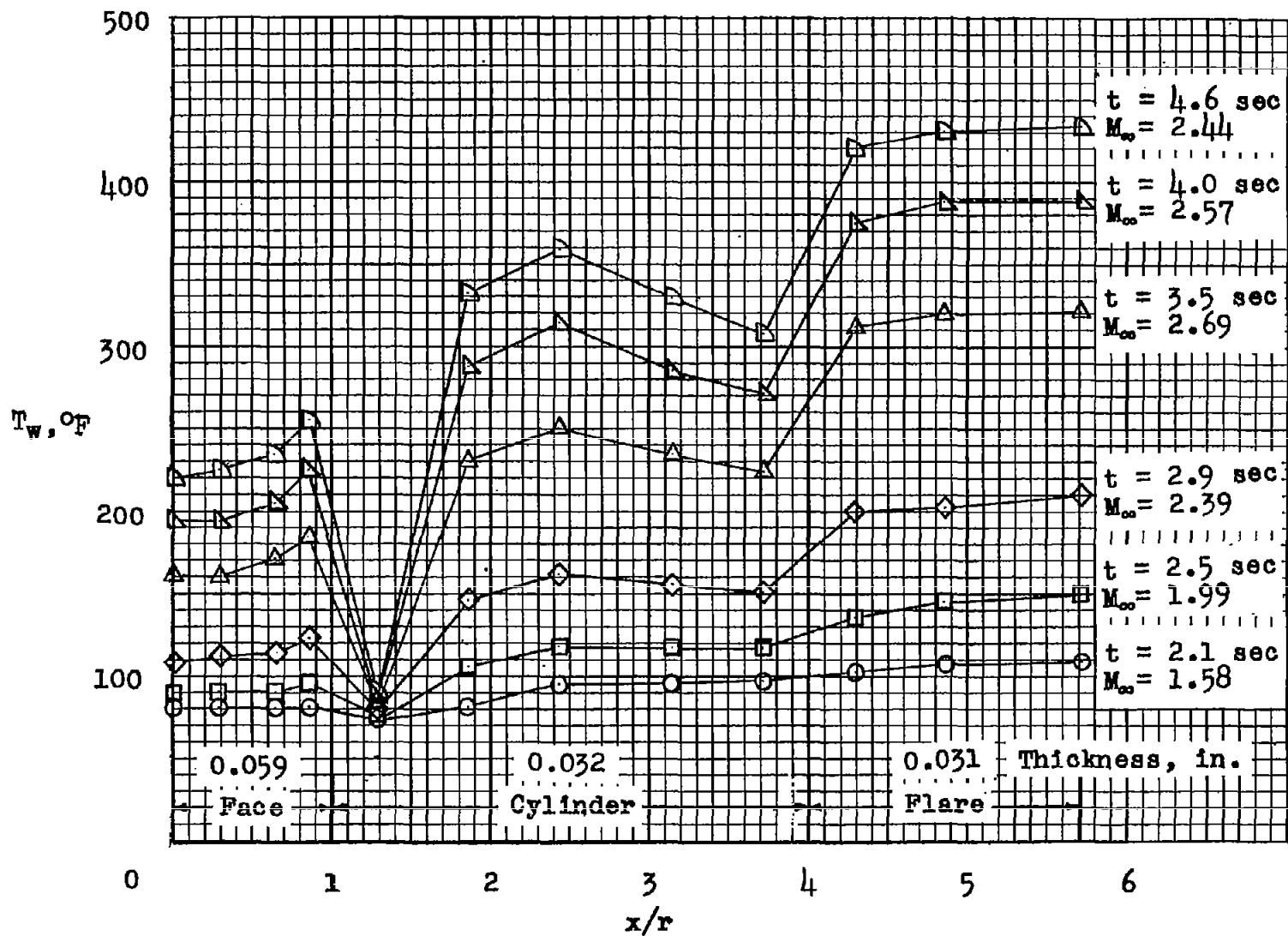
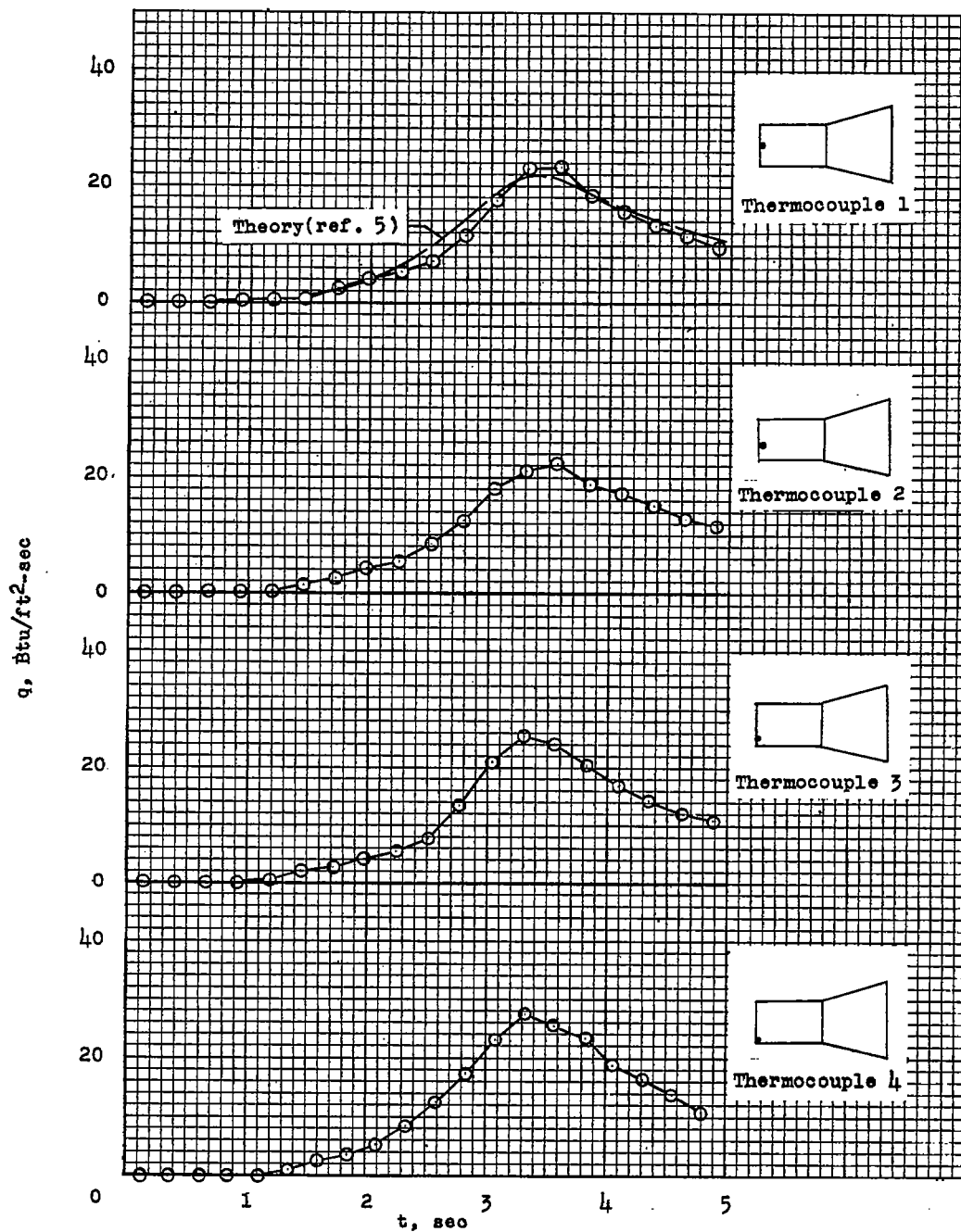
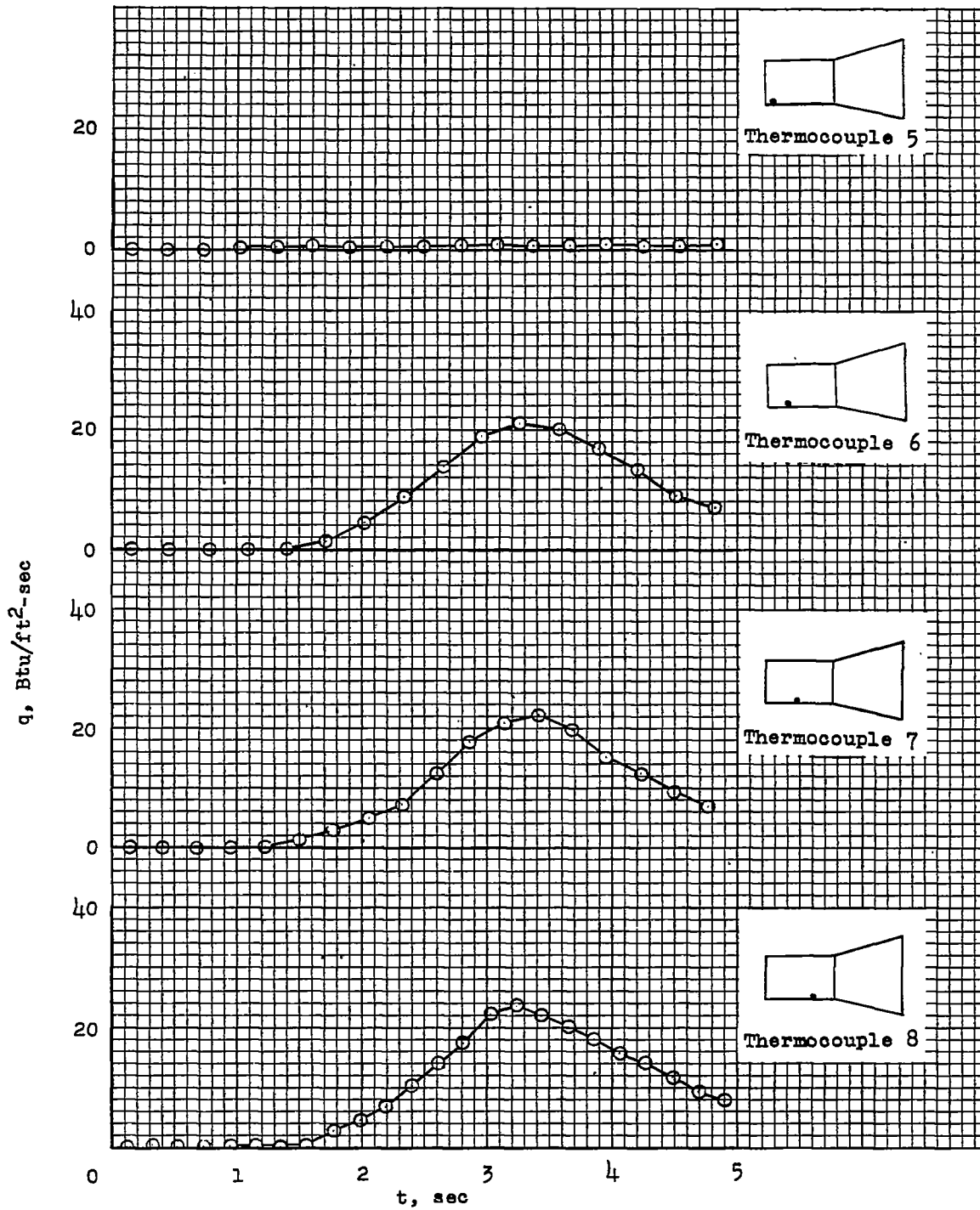


Figure 7.- Distribution of outside temperatures along the nose.



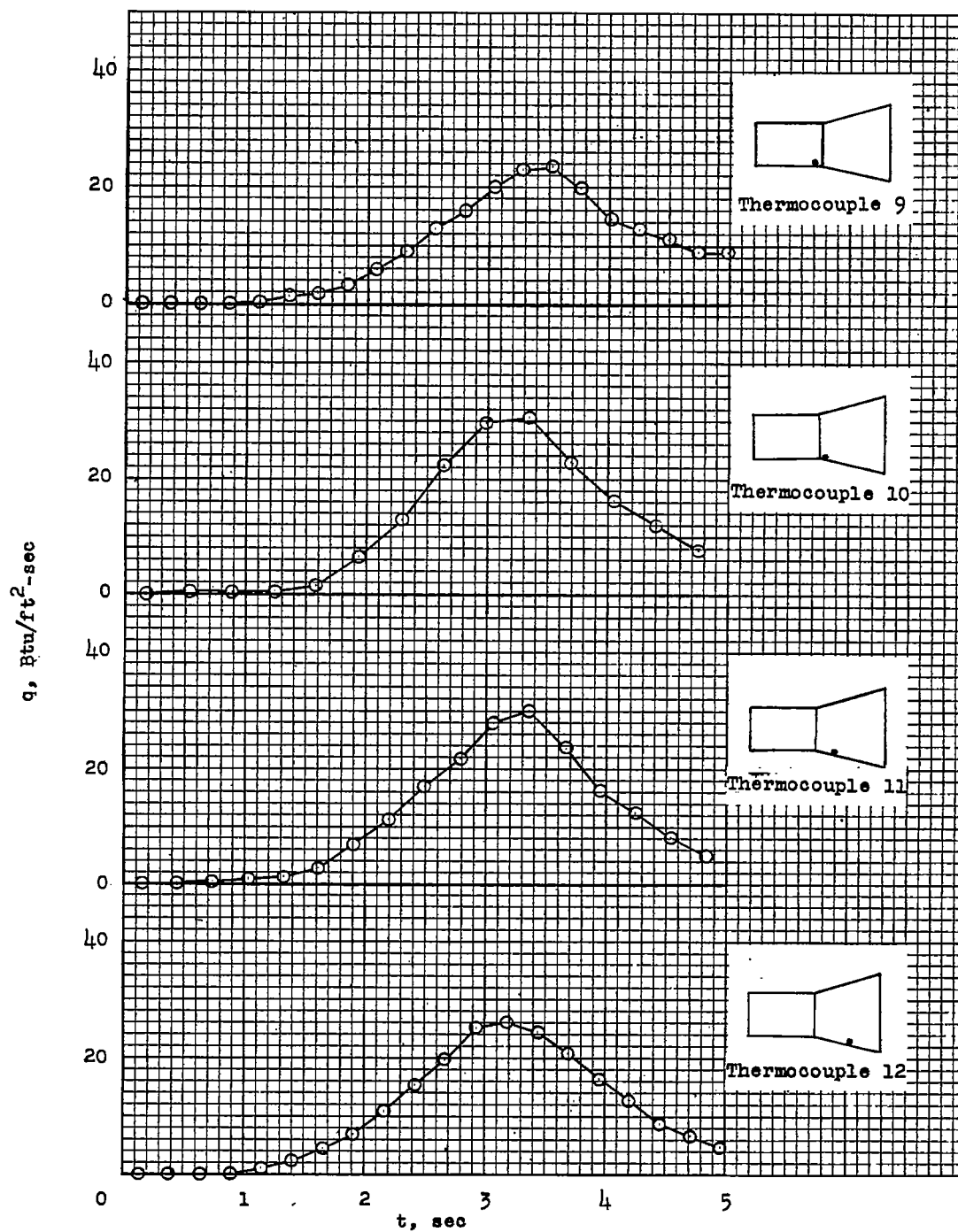
(a) Measured heating rates on the flat face.

Figure 8.- Time histories of heating rates for each thermocouple location on the nose.



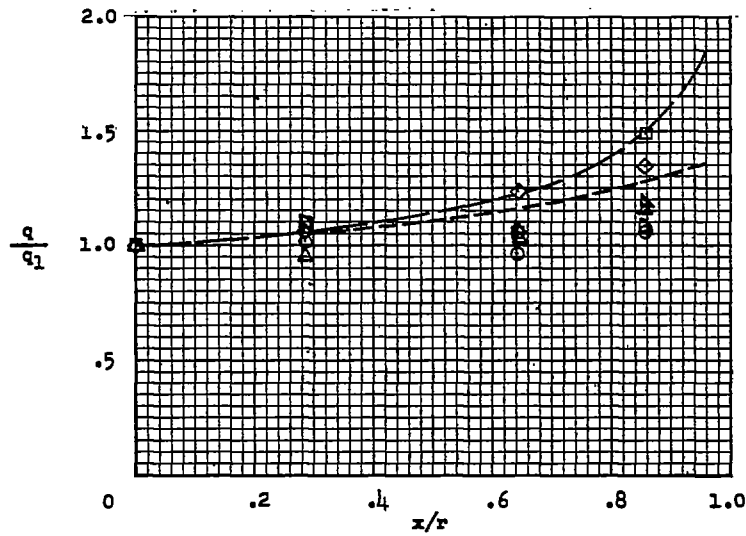
(b) Measured heating rates on the cylinder.

Figure 8.- Continued.

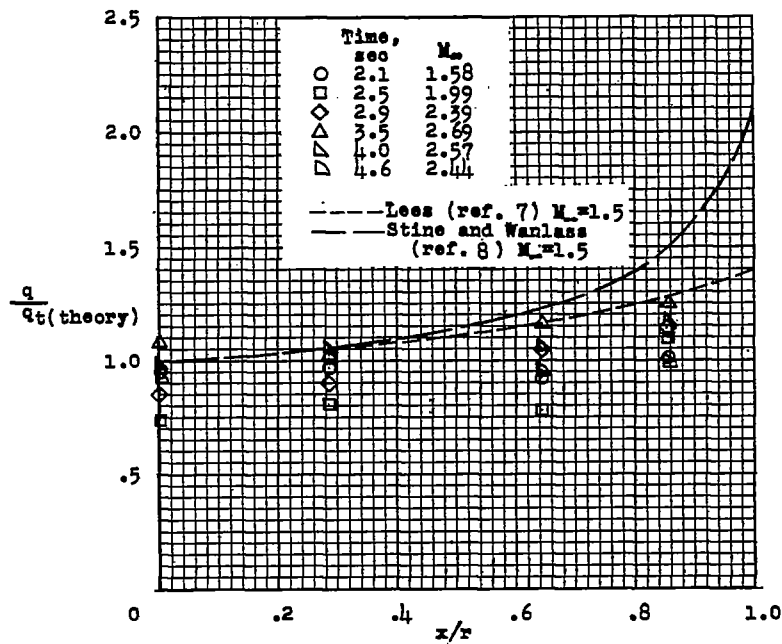


(c) Measured heating rates on the cylinder and flare.

Figure 8.- Concluded.



(a) Experimental heating rates divided by the measured stagnation point heating rate.



(b) Experimental heating rates divided by the theoretical stagnation point heating rate.

Figure 9.- Distribution of heating rate ratios along the flat face.

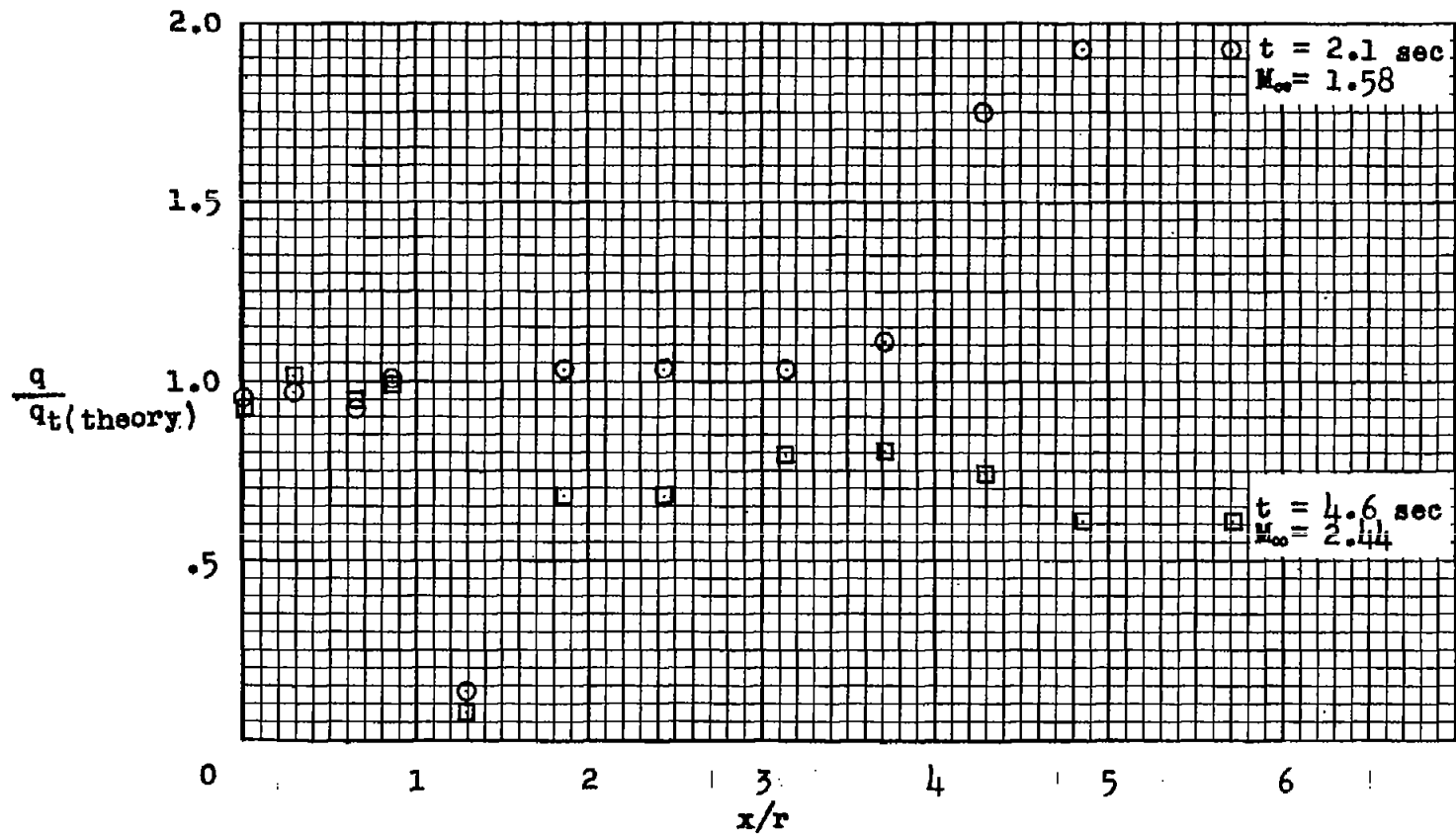
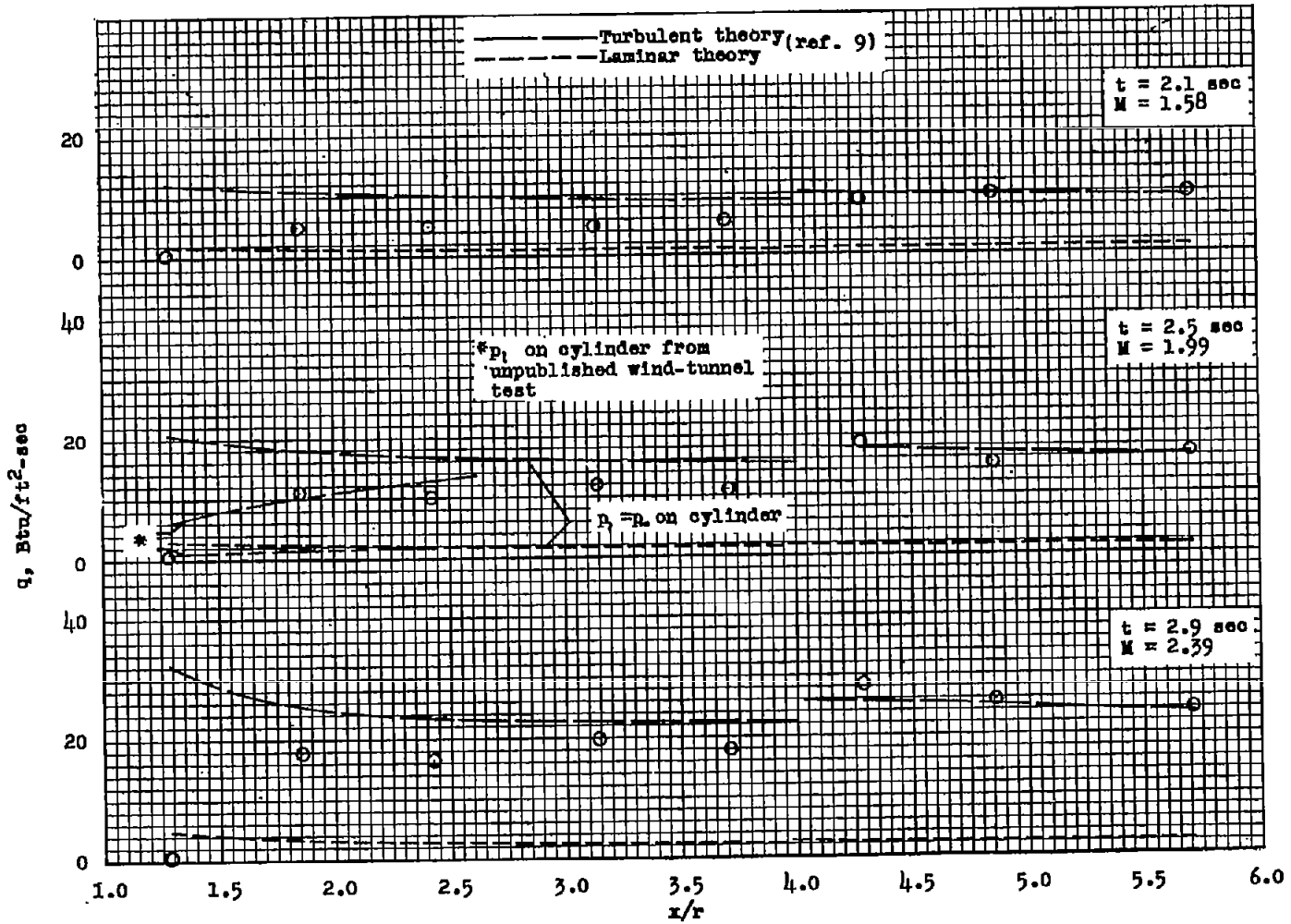


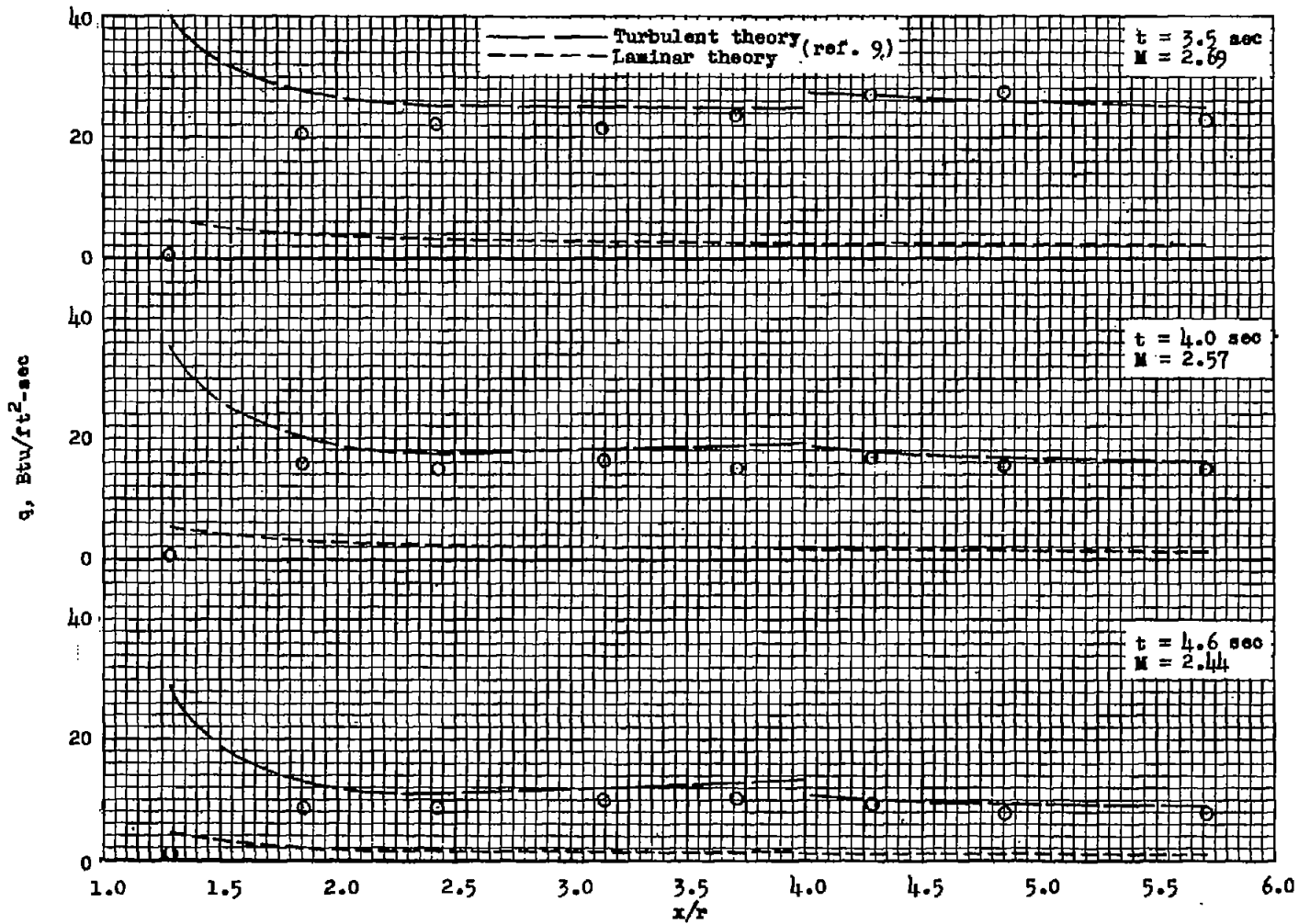
Figure 10.- Distribution along the nose of the ratios of experimental heating rates to stagnation theoretical heating rates.

CONFIDENTIAL



(a) For times 2.1, 2.5, and 2.9 seconds.

Figure 11.- Comparison of experimental with turbulent and laminar theoretical heating rates along the cylinder and flare of the nose.



(b) For times 3.5, 4.0, and 4.6 seconds.

Figure 11.- Concluded.

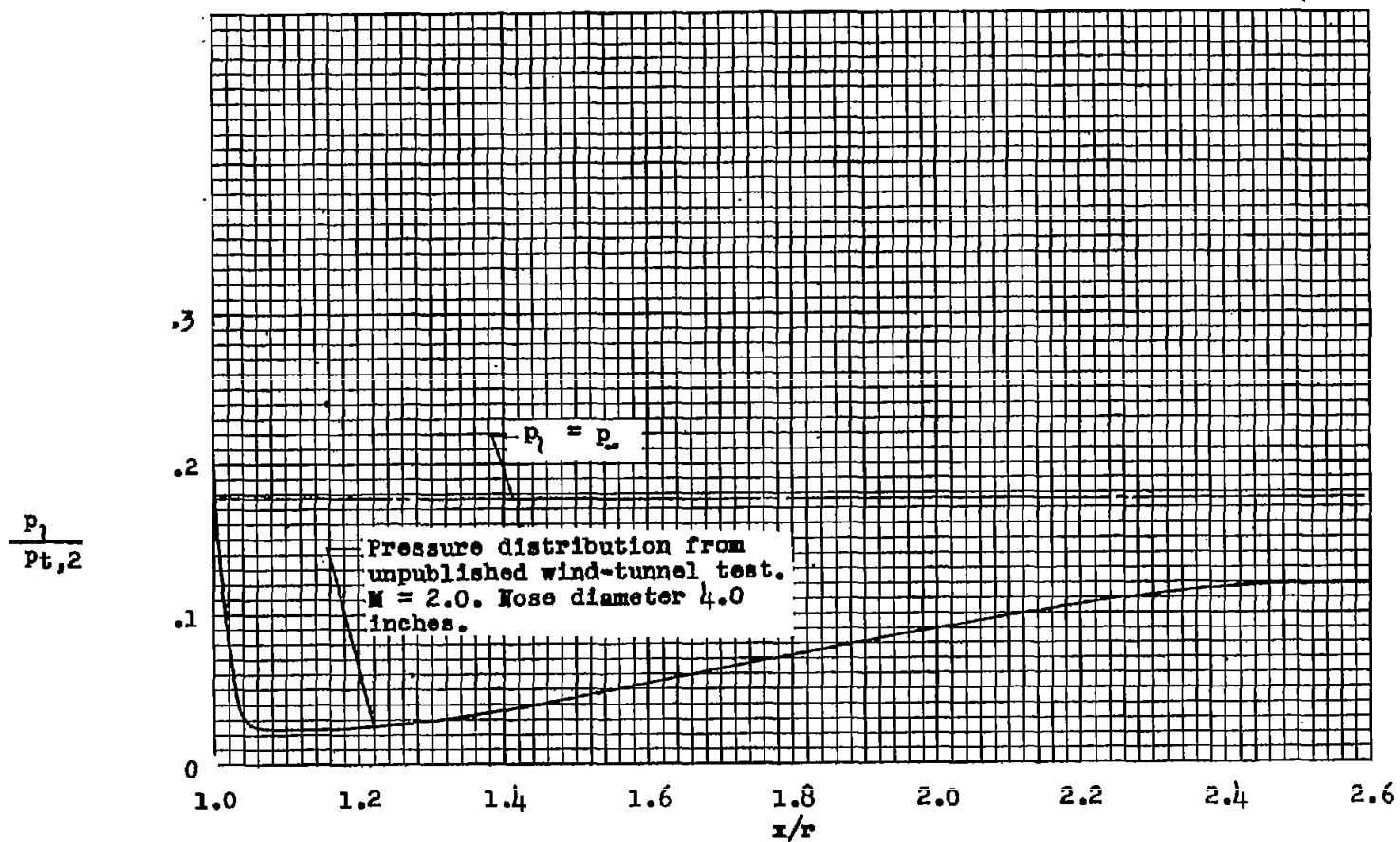
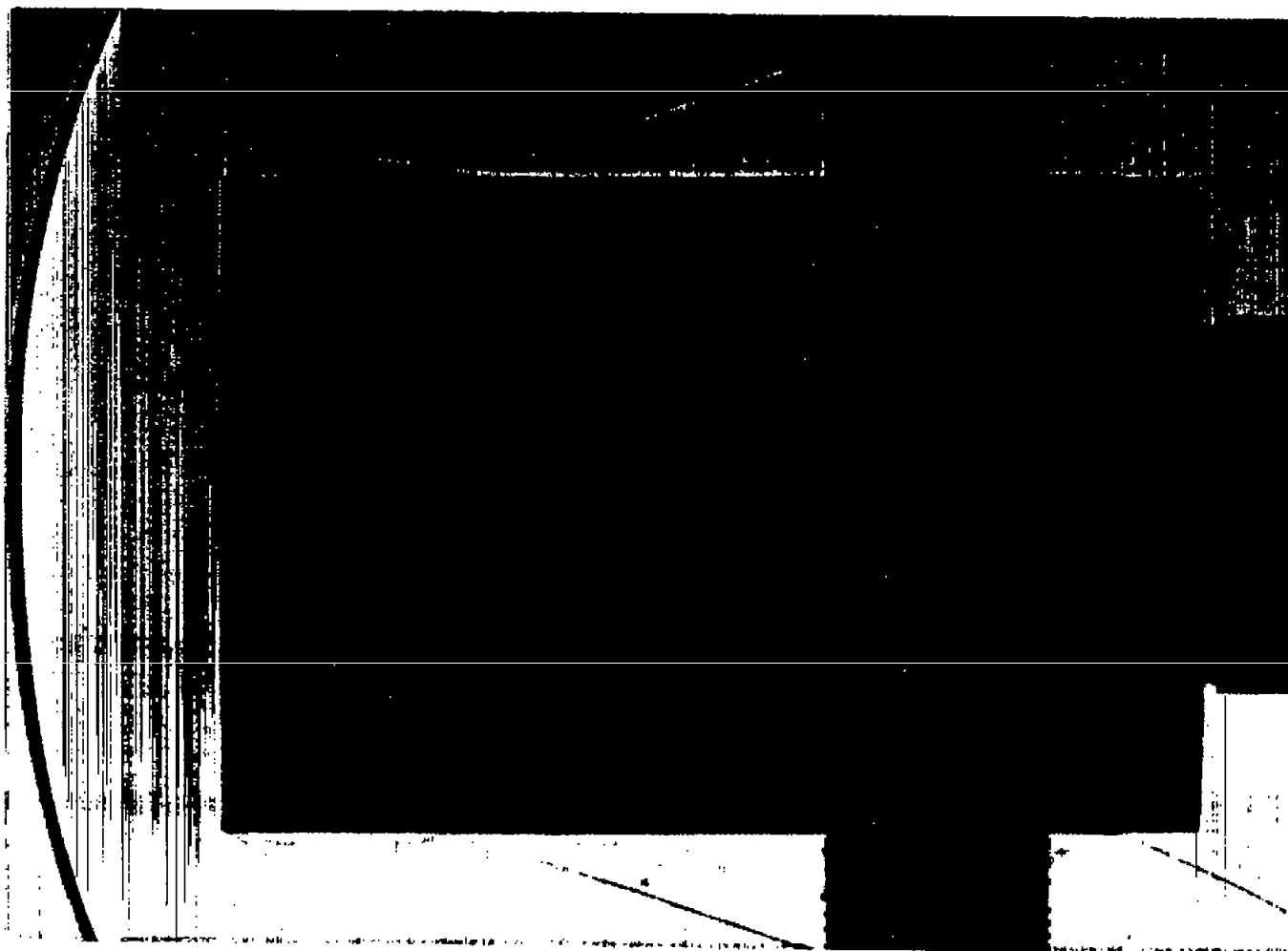


Figure 12.- Distribution along the cylinder of local pressure divided by the total pressure behind a normal shock.



L-57-4454
Figure 13.- Shadowgraph of flow around blunt-nosed cylinder showing separated flow at corner
obtained from unpublished wind-tunnel test.

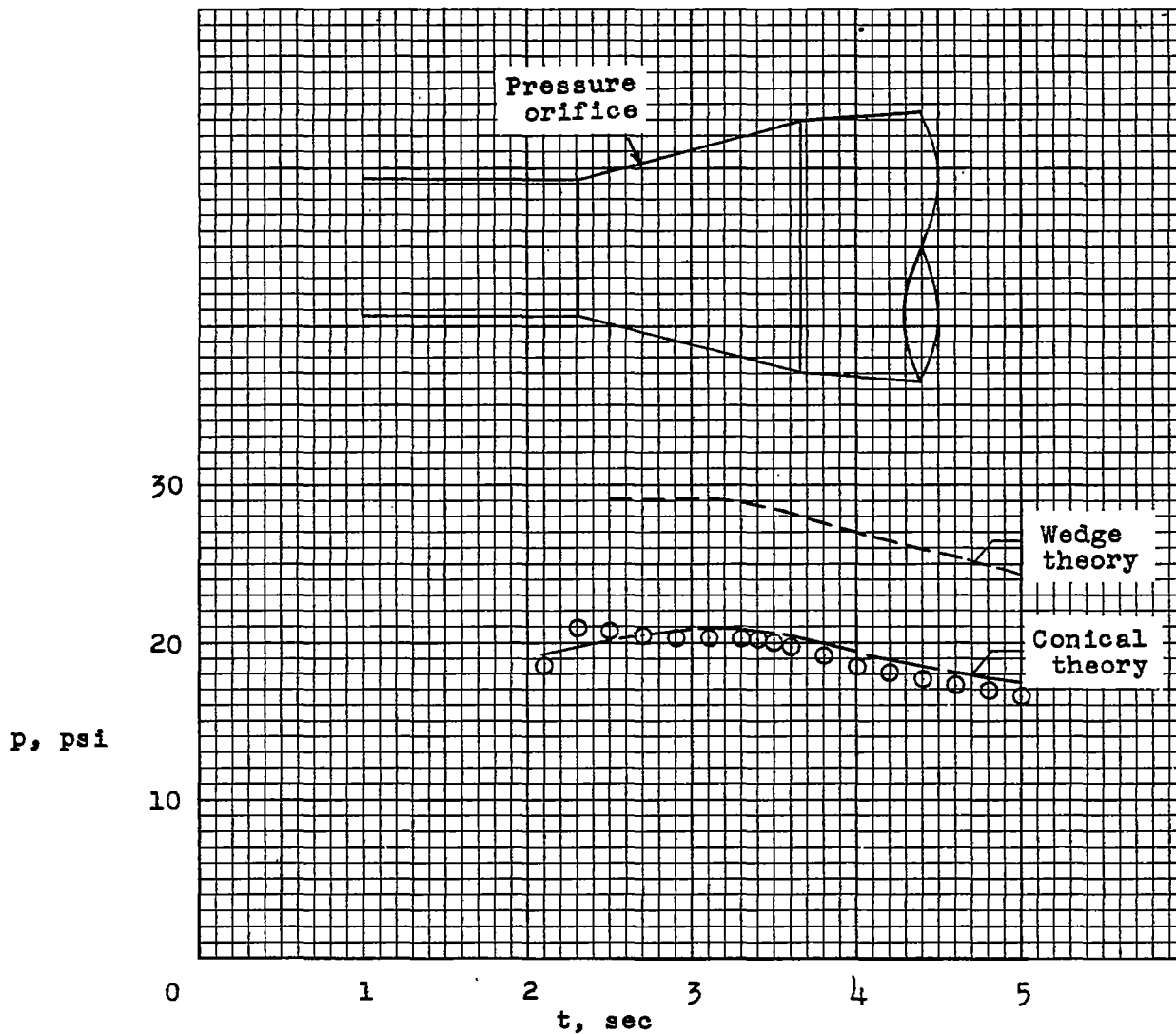


Figure 14.- Time histories of experimental and computed theoretical pressures.